

Calculation of the surface tension from multibody dissipative particle dynamics and Monte Carlo methods

A. Ghoufi

Institut de Physique de Rennes, UMR 6251 CNRS, Université Rennes 1, 263 avenue du Général Leclerc, 35042 Rennes

P. Malfreyt*

Clermont Université, Université Blaise Pascal, Laboratoire de Thermodynamique et Interactions Moléculaires, CNRS, UMR 6272, LTIM, BP 10448, F-63000 CLERMONT-FERRAND

(Received 29 March 2010; revised manuscript received 14 June 2010; published 19 July 2010)

We report the calculation of the coexisting densities and surface tensions of the liquid-vapor equilibrium using the multibody dissipative particle dynamics and Monte Carlo (MMC) methods. We focus on the calculation of the surface tension by using the thermodynamic and mechanical routes. It is the first time that the test-area method is applied on the many-body conservative potential. We discuss the mechanical equilibrium of these two-phase systems by analyzing the profiles of the normal and tangential components of the pressure tensor using the Irving-Kirkwood and Kirkwood-Buff approaches. The profile of the configurational temperature is shown to establish the thermal equilibrium of these two-phase simulations carried out with large time steps. We complete this study to show the impact of the range of the many-body repulsive term of the conservative force on the surface tension. We conclude that the MMC method is an efficient sampling scheme to compute the interfacial properties of liquid-vapor interfaces using the multibody soft potential.

DOI: [10.1103/PhysRevE.82.016706](https://doi.org/10.1103/PhysRevE.82.016706)

PACS number(s): 02.70.-c, 68.03.-g

I. INTRODUCTION

The mesoscale modeling consists of covering length and time scales which are intermediate between the atomic length scale and the macroscopic length scale. The modeling at this scale, 10–100 nm and 1 ns–10 μ s requires to introduce a coarse graining of the microscopic degrees of freedom. This should allow to study larger-scale systems for longer times. The dissipative particle dynamics (DPD), proposed by Hoogerbrugge and Koelman [1,2] is a genuinely mesoscale approach for studying the behavior of simple and complex fluids. DPD is a stochastic dynamics method in which the individual particles (beads) represent a set of atomistic degrees of freedom. As a consequence of this coarse graining, the conservative interactions are soft [3]. The dissipative and Brownian forces are short-ranged and pairwise additive so that the hydrodynamics of the fluid satisfies the Navier-Stokes equation. There are two major advantages to the DPD method. First, the soft potential allows for a time step that is up to an order of magnitude larger than those typically used in molecular dynamics (MD) simulations. Second, the method, unlike the Brownian dynamics technique, includes a correct description of hydrodynamic interactions.

The original version of the DPD methodology has received substantial theoretical support concerning the extension of the DPD for the conservation of the total energy [4–6], the incorporation of the electrostatic interactions [7–10] and the modeling of entanglements by avoiding bond crossings [11,12]. The so-called multibody DPD method (MDPD) has also been established [13–16] to model liquid-vapor interfaces. Within this method, the conservative inter-

actions are modified by an additional contribution which is dependent on the local density.

The thrust of our research is to use the MDPD simulations to calculate the surface tension of liquid-vapor interface of real fluids by fitting the DPD parameters on specific atomistic parameters. But, before doing so, we have to check different fundamental points concerning the surface tension calculation with the MDPD method.

From a molecular viewpoint, we have already successfully used the Monte Carlo (MC) simulations methods in order to reproduce the dependence of the surface tension with temperature for linear and branched alkanes [17–21], cyclic and aromatic hydrocarbons [22–24], water and acid gases [25–29]. It was also established that the molecular simulations of two-phase systems can be sensitive to a certain number of factors such as the finite size effects [30–33], the range of interactions [18,34–36], the truncation effects [12,20,34,37] and the method used (MC and MD) [34,37]. The surface tension calculation is based upon the mechanical and thermodynamic definitions [20,27,38]. A certain number of operational expressions have been established for the surface tension calculation. The most general working expression uses macroscopic normal and tangential pressures which can be related to the derivative of the pair potential. The final form has been obtained by Kirkwood and Buff [39–42] (KB) and gives a macroscopic scalar surface tension. In the case of a planar liquid-vapor interface lying in the x,y plane, the density gradient takes place in the z direction normal to the surface. The surface tension can be expressed as $\int_{-\infty}^{\infty} [p_N(z) - p_T(z)] dz$ where $p_N(z)$ and $p_T(z)$ are the average local values of the normal and tangential components of the pressure tensor, respectively. Expressing the surface tension as a function of the local components of the pressure allows to use a local property defined as $\int_{-\infty}^z [p_N(z') - p_T(z')] dz'$. The use of this local value is a key element to check the validity of the

*patrice.malfreyt@univ-bpclermont.fr

calculation concerning the stabilization of the interfaces, the independence between the two interfaces (for a three dimensionally periodic system) and the constancy of the difference between the normal and tangential pressure profiles in the bulk phases. We note that there are many ways of expressing the local components of the pressure which depend on the contour joining two interacting molecules. Irving and Kirkwood [43–46] (IK) use a straight line to join the two particles. This choice is the most natural and the one generally made. Nevertheless, the scalar value of surface tension is invariant to the choice of the pressure tensor. Until recently, only the method of Irving and Kirkwood was designed to provide a profile of the surface tension. Both methods (KB, IK) are based upon the mechanical definition on the surface tension. Recently, the “test-area” [38] (TA) method based upon the perturbation formalism was proposed for the calculation of the surface tension. This method takes advantage of expressing the surface tension as a difference of energy between a reference state and a perturbed state characterized by an infinitesimal increase or decrease of the surface. However, the aspect of the local surface tension was missing within the Kirkwood-Buff expression and the test-area (TA) method. This led us to establish the local expression of the surface tension calculated from the test-area approach [20] and to propose the local version of the surface tension resulting from the virial route (KBZ) in a recent work [27]. The long range corrections to the surface tension are now well-established and have been reported for each definition [18,20,27,37,47,48].

The aim of this work is to investigate the calculation of the local normal and tangential pressures in the liquid-vapor interface using the MDPD simulations. We will focus on the calculation of the surface tension from the different definitions and we will compare the different results between the MDPD and the MC simulations carried out with the many-body model. These comparisons constitute prerequisite results before an extension of this model to molecular systems. The paper is organized as follows. Section II contains the description of the many-body DPD methodology and of the Hamiltonian used in the Monte Carlo simulations. Section III describes the computational procedures and the different definitions of the surface tension calculation are given in Sec. IV. Our results are presented in Sec. V. Section VI contains the main conclusions drawn from this work.

II. DPD METHODOLOGY

A. Standard dissipative particle dynamics (DPD) method

In the DPD approach, particles are coarse grained into soft beads that interact with the pairwise additive force \mathbf{f}_i defined as the sum of three contributions

$$\mathbf{f}_i = \sum_{j \neq i} (\mathbf{f}_{ij}^C + \mathbf{f}_{ij}^R + \mathbf{f}_{ij}^D), \quad (1)$$

where \mathbf{f}_{ij}^C , \mathbf{f}_{ij}^R , and \mathbf{f}_{ij}^D are the conservative, random and dissipative forces, respectively. The conservative repulsive force \mathbf{f}_{ij}^C derives from a soft interaction potential and is expressed as follows:

$$\mathbf{f}_{ij}^C = \begin{cases} a_{ij} \omega_C(r_{ij}) \mathbf{e}_{ij} & (r_{ij} < r_c) \\ 0 & (r_{ij} \geq r_c) \end{cases}, \quad (2)$$

where a_{ij} is the maximum repulsion parameter between particles i and j , r_{ij} is the relative displacement of particles i and j and \mathbf{e}_{ij} is the corresponding unit vector. The standard DPD model uses a repulsive conservative force ($a_{ij} > 0$). The weight function $\omega_C(r_{ij})$ is equal to $1 - r_{ij}/r_c$ for $r_{ij} \leq r_c$ and vanishes for $r_{ij} \geq r_c$. The dissipative and random forces are given by

$$\mathbf{f}_{ij}^D = -\gamma \omega^D(\mathbf{e}_{ij} \times \mathbf{v}_{ij}) \mathbf{e}_{ij}, \quad (3)$$

$$\mathbf{f}_{ij}^R = \sigma \omega^R \theta_{ij} \frac{1}{\sqrt{\delta t}} \mathbf{e}_{ij}, \quad (4)$$

where δt is the time step. $\mathbf{v}_{ij} = \mathbf{v}_i - \mathbf{v}_j$ is the relative velocity, σ is the amplitude of the noise, θ_{ij} is a random Gaussian number with zero mean and unit variance. γ and σ are the dissipation strength and noise strength, respectively. The terms $\omega^D(r_{ij})$ and $\omega^R(r_{ij})$ are dimensionless weighting functions. Español and Warren [49] have shown that the system will sample the canonical ensemble and obey the fluctuation-dissipation theorem if the following conditions are satisfied:

$$\gamma = \frac{\sigma^2}{2k_B T} \quad \text{and} \quad \omega^D(r_{ij}) = [\omega^R(r_{ij})]^2, \quad (5)$$

where k_B is Boltzmann’s constant and T is the temperature. The weighting function $\omega^R(r_{ij})$ is chosen to be similar to $\omega^C(r_{ij})$.

B. Many-body dissipative particle dynamics (MDPD) method

Within the many-body DPD technique, the conservative force [13–16] is not only dependent on the interparticle separation but also on the local particle density. The resulting conservative force is then expressed as

$$\mathbf{f}_{ij}^C = a_{ij} \omega_C(r_{ij}) \mathbf{e}_{ij} + b_{ij} [\bar{\rho}_i + \bar{\rho}_j] \omega_d(r_{ij}) \mathbf{e}_{ij}, \quad (6)$$

where the first term of Eq. (6) represents an attractive interaction ($a_{ij} < 0$) and the second many-body term a repulsive interaction ($b_{ij} > 0$). This is in line with the formalism used by Warren [15]. The weight function $\omega_d(r_{ij})$ in Eq. (6) is chosen as

$$\omega_d(r_{ij}) = \begin{cases} 1 - \frac{r_{ij}}{r_d} & \text{if } r_{ij} < r_d \\ 0 & \text{if } r_{ij} > r_d \end{cases}, \quad (7)$$

where r_d defines the range of the repulsive many-body interaction with $r_d < r_c$ and $\bar{\rho}_i$ represents the average local density at the position of the particle i defined as

$$\bar{\rho}_i = \sum_{j \neq i} \omega_\rho(r_{ij}). \quad (8)$$

The weight function $\omega_\rho(r_{ij})$ is normalized so that $\int_0^\infty 4\pi r^2 \omega_\rho(r) dr = 1$. Its operational expression becomes

$$\omega_\rho(r_{ij}) = \begin{cases} \frac{15}{2\pi r_d^3} \left(1 - \frac{r_{ij}}{r_d}\right)^2 & \text{if } r_{ij} < r_d \\ 0 & \text{if } r_{ij} > r_d \end{cases}. \quad (9)$$

C. Multibody Monte Carlo (MMC) simulations

MC simulation aims to explore the configurational space of a system using the calculation of changes in the intermolecular energy. We need then the potential function that gives rise to the expression of the conservative force given in Eq. (6). By integrating the conservative force $\mathbf{f}_i^C = \sum_{j \neq i} \mathbf{f}_{ij}^C$, we obtain the energy u_i^C of a particle i defined as

$$U^C = \sum_i u_i^C = \sum_i \left(\frac{\pi r_c^3}{30} A \sum_{j \neq i} \omega_\rho(r_{ij}, R = r_c) + \frac{\pi r_d^4}{30} B \left[\sum_{j \neq i} \omega_\rho(r_{ij}, R = r_d) \right]^2 \right), \quad (10)$$

where the $\omega_\rho(r_{ij}, R)$ is a generalized weight function of range R defined as

$$\omega_\rho(r_{ij}, R) = \begin{cases} \frac{15}{2\pi R^3} \left(1 - \frac{r_{ij}}{R}\right)^2 & \text{if } r_{ij} < R \\ 0 & \text{if } r_{ij} > R \end{cases}. \quad (11)$$

In the case of one component fluid system, A and B correspond to the a_{ij} and b_{ij} energy parameters, respectively. The MMC simulations use the potential of Eq. (10) that requires the calculation of the local density of each particle at each MC move. For a better efficiency in the calculation of the local density, we use the linked cell method. It consists in the partition of the simulation box into smaller cells, each of them with dimensions slightly larger than the reduced cutoff. With this algorithm, the interactions between a given particle and its neighbors can be calculated by considering the particles that are in its same cell or in the 26 other linked cells surrounding it.

III. SIMULATION DETAILS

Usually, all the DPD particles have the same mass. The mass of a particle is taken as unity, as well as the cutoff radius r_c . Consequently, the reduced length is expressed as $r^* = r/r_c$ and the reduced density is $\rho^* = (N/V)r_c^{-3}$. The reduced temperature is defined as $T^* = k_B T / \epsilon$ where ϵ sets the energy scale. The other reduced variables can then be deduced, like the interaction parameter $a^* = a(r_c/\epsilon)$, the unit of time $t^* = t(\epsilon/mr_c^2)^{1/2}$ and the surface tension $\gamma^* = \gamma(r_c^2/\epsilon)$. Reduced units are a convenient tool for DPD. As all the values presented here are in reduced units, the star notation is omitted in the following for clarity.

The initial configuration of the liquid-vapor interface system was prepared from bulk phase configurations of the DPD fluid. The cell parameters of the bulk configurations were set to have the same L_x and L_y dimensions ($L_x = L_y = 8$). The dimension of the resulting box was increased along the z axis by placing two empty cells on both sides of the bulk fluid

box. The L_z dimension was chosen to be five times higher than L_x in order to avoid a dependence of the surface tension with L_z as it was established in a previous paper [33]. The choice of $L_x = L_y = 8$ is also based upon consideration of size effects. In fact, it was demonstrated [50] that from such values of interfacial area the surface tension of mixture of two DPD fluids becomes independent of the interfacial area and that the stress anisotropy in the bulk phase vanishes. Periodic boundary conditions were applied in the three directions. The total number of particles was 3072.

The energy parameters for all the simulations were fixed to $a_{ij} = A = -40$ and $b_{ij} = B = 40$ and the cutoff radius r_d was fixed to 0.75. The $k_B T$ temperature was changed from 1 to 2.5. The equations of motions of the MDPD simulations were integrated using a modified velocity-Verlet algorithm. The time step was $\delta t = 0.001$. The random and dissipative parameters were $\sigma = 3$ and $\gamma = 4.5$. The equilibration phase was formed by 500 000 steps and the average thermodynamic properties were averaged over 10^6 additional steps. Monte Carlo simulations were performed in the NVT ensemble. Each cycle consisted of N translation moves of the particles. The maximum displacement is obtained such that 40% of the translation moves are accepted. The number of cycles was equal to 500 000 for the equilibration phase and additional 500 000 cycles for the production phase. As the geometry of the system shows a heterogeneity along the axis normal to the interface (z axis), we expect a dependence of the thermodynamic properties only in this direction. We have therefore calculated the temperature, pressure, and surface tension as a function of z by splitting the cell into slabs of width Δz . Δz was fixed to 0.5 for the profile calculation.

IV. SURFACE TENSION AND PRESSURE CALCULATIONS

Surface tension can be computed using the thermodynamic [38] and mechanical [39,44] definitions. The thermodynamic route uses the test-area (TA) [38] whereas the mechanical route uses the Irving-Kirkwood definition [44] and Kirkwood Buff definition [39]. The long range corrections to the thermodynamic properties are not required because the force and potential vanish at the cutoff radius.

A. Tensorial components of the pressure

For a homogeneous fluid assuming pairwise interactions, the components of the pressure tensor can be defined as

$$P_{\alpha\beta} = \langle \rho \rangle k_B T \delta_{\alpha\beta} + \frac{1}{V} \left\langle \sum_{i=1}^{N-1} \sum_{j>i}^N (\mathbf{r}_{ij})_\alpha (\mathbf{f}_{ij}^C)_\beta \right\rangle, \quad (12)$$

where α and β represent x , y , or z directions. $\delta_{\alpha\beta}$ is the Kronecker delta, $(\mathbf{r}_{ij})_\alpha$ is the α component of the particle vector \mathbf{r}_{ij} . $(\mathbf{f}_{ij}^C)_\beta$ is the β component of the force \mathbf{f}_{ij}^C between particle i and j . For an inhomogeneous system, the pressure depends on the position \mathbf{r} in the fluid. The first term is a kinetic contribution from the momentum of the particles. The second term is the configurational or potential part of the pressure arising from the conservative forces between the particles. It is subjected to arbitrariness because there is no

unique way to determine which pairs of particle contribute to the virial at a given \mathbf{r} . The α - β component of the pressure tensor [51] at a given \mathbf{r} becomes

$$p_{\alpha\beta}(\mathbf{r}) = \langle \rho(\mathbf{r}) \rangle k_B T \delta_{\alpha\beta} + \left\langle \sum_{i=1}^{N-1} \sum_{j>i}^N (\mathbf{r}_{ij})_{\alpha} (\mathbf{f}_{ij}^C)_{\beta} \xi_{\alpha\beta}(\mathbf{r}, \mathbf{r}_i, \mathbf{r}_j) \right\rangle, \quad (13)$$

where the double sum is restricted to the pairs of particle that contribute to the virial component at a given fixed position \mathbf{r} . $\xi_{\alpha\beta}(\mathbf{r}, \mathbf{r}_i, \mathbf{r}_j)$ is defined as the fraction of the virial between a particle i at \mathbf{r}_i and a particle j at \mathbf{r}_j to be assigned to position \mathbf{r} . This function must satisfy the following normalization condition:

$$\int d\mathbf{r} \xi_{\alpha\beta}(\mathbf{r}, \mathbf{r}_i, \mathbf{r}_j) = 1, \quad (14)$$

where the integration is carried out over the volume of the simulation cell. When the system is homogeneous, the virial is distributed over the whole system and $\xi_{\alpha\beta}(\mathbf{r}, \mathbf{r}_i, \mathbf{r}_j) = 1/V$ and Eq. (13) is equivalent to Eq. (12).

When the simulation shows a liquid-vapor interface along the z direction, the components of the pressure tensor depend on the distance z from the surface. $\xi_{\alpha\beta}$ is then defined as

$$\xi_{\alpha\beta}(\mathbf{r}, \mathbf{r}_i, \mathbf{r}_j) = \frac{1}{A} \xi_{\alpha\beta}(z, z_i, z_j), \quad (15)$$

where $\xi_{\alpha\beta}(z, z_i, z_j)$ corresponds to the fraction of virial between a pair of particles at positions z_i and z_j to be assigned to the slab at position z . This slab has a surface area $A = L_x L_y$. The normalization conditions for $\xi_{\alpha\beta}(z, z_i, z_j)$ requires that

$$\int dz \xi_{\alpha\beta}(z, z_i, z_j) = 1. \quad (16)$$

The α - β component of the pressure tensor along the z direction can be thus written as

$$p_{\alpha\beta}(z) = \langle \rho(z) \rangle k_B T \delta_{\alpha\beta} + \frac{1}{A} \left\langle \sum_{i=1}^{N-1} \sum_{j>i}^N (\mathbf{r}_{ij})_{\alpha} (\mathbf{f}_{ij}^C)_{\beta} \xi_{\alpha\beta}(z, z_i, z_j) \right\rangle \quad (17)$$

B. Irving-Kirkwood (IK) definition

The method of Irving and Kirkwood [44] (IK) is based upon the notion of the force across a unit area. With this definition [43,45,52], only the pairs of particles for which the vector $\mathbf{r}_{ij} = \mathbf{r}_j - \mathbf{r}_i$ passes through the surface element dA contribute to the stress across dA . This definition [43,45,52] leads to an even distribution of the virial among all planes z between z_i and z_j for the normal and tangential components of the pressure tensor. This implies that

$$\xi_N = \xi_T(z, z_i, z_j) = \int_0^1 d\alpha \delta(z - z_i - \alpha z_{ij}) \quad (18)$$

$$= \frac{1}{|z_{ij}|} \theta\left(\frac{z - z_i}{z_{ij}}\right) \theta\left(\frac{z_j - z}{z_{ij}}\right), \quad (19)$$

where $\alpha = (z - z_i)/z_{ij}$, $\delta(x)$, and $\theta(x)$ are the Dirac delta and Heaviside functions, respectively.

The components of the pressure tensor [43,45,52] in the Irving and Kirkwood definition are thus given by

$$p_{\alpha\beta}(z) = \langle \rho(z) \rangle k_B T \mathbf{I} + \frac{1}{A} \left\langle \sum_{i=1}^{N-1} \sum_{j>i}^N (\mathbf{r}_{ij})_{\alpha} (\mathbf{f}_{ij}^C)_{\beta} \frac{1}{|z_{ij}|} \theta\left(\frac{z - z_i}{z_{ij}}\right) \theta\left(\frac{z_j - z}{z_{ij}}\right) \right\rangle, \quad (20)$$

where \mathbf{I} is the unit tensor and $k_B T$ is the input temperature and \mathbf{f}_{ij}^C is the conservative force defined in Eq. (6). Following Irving and Kirkwood, the particles i and j give a local contribution to the stress across the plane placed at z if the line joining the particles i and j crosses, starts or finishes in the plane. The normal component $p_N(z_k)$ is equal to $p_{zz}(z)$ whereas the tangential component is given by $\frac{1}{2}[p_{xx}(z) + p_{yy}(z)]$.

The surface tension is then expressed from the local components of the pressure tensor as

$$\gamma_{IK} = \frac{1}{2} \int_{-L_z/2}^{L_z/2} [p_N(z) - p_T(z)] dz \quad (21)$$

An other method called ‘‘method of planes’’ [53] avoiding the ambiguity of defining a contour to relate two particles was proposed to calculate the pressure tensor. However, this method does not allow for the calculation of the tangential components of the pressure tensor. As a result, the calculation of the surface tension is not possible with this method.

C. Macroscopic (KB) and local (KBZ) versions of the Kirkwood Buff definition

The surface tension γ_{KB} , first introduced by Kirkwood and Buff [39], is given by

$$\gamma_{KB} = \frac{1}{2A} \left\langle \sum_{i=1}^{N-1} \sum_{j=i+1}^N \left(\frac{3z_{ij} \cdot z_{ij} - \mathbf{r}_{ij} \cdot \mathbf{r}_{ij}}{2r_{ij}} \right) f_{ij}^C(r_{ij}) \right\rangle. \quad (22)$$

In a previous work, we established a local version [27] of the surface tension based upon the KB expression. The working expression was obtained from the derivative of the potential with the respect to the surface and can be written as

$$\gamma_{KBZ} = \left\langle \frac{\partial U}{\partial A} \right\rangle = \sum_k^{N_s} \left\langle \frac{\partial U_z}{\partial A} \right\rangle = \sum_k^{N_s} \gamma_{KBZ}(z)$$

where N_s is the number of slabs of width Δz along the z direction. $\gamma_{KBZ}(z)$ is defined as

$$\gamma_{KBZ}(z) = \left\langle \frac{\partial U_z}{\partial A} \right\rangle = \left\langle \sum_i \sum_{j \neq i} H(z) f_{ij}^C(r_{ij}) \left(\frac{3z_{ij}^2 - r_{ij}^2}{2r_{ij}} \right) \right\rangle, \quad (23)$$

where $H(z_i)$ is a top-hat function with functional values of

$$\begin{cases} H(z_i) = 1 & \text{for } z - \frac{\Delta z}{2} < z_i < z + \frac{\Delta z}{2} \\ H(z_i) = 0 & \text{otherwise} \end{cases}. \quad (24)$$

Within the KBZ definition, it is possible to define the components of the pressure tensor. These components correspond to those obtained from the IK1 definition [53,45] which derives from the tensorization of the full IK method using the Harasima [55] contour. The components of the pressure calculated using the IK1 or KBZ methods can be calculated from

$$p_{\alpha\beta}(z) = \langle \rho(z) \rangle k_B T \mathbf{I} + \frac{1}{A} \left\langle \sum_{i=1}^{N-1} \sum_{j>i}^N H(z_i) f_{ij}^C \left(\frac{(\mathbf{r}_{ij})_\alpha (\mathbf{r}_{ij})_\beta}{r_{ij}} \right) \right\rangle. \quad (25)$$

D. Test area (TA) method

The test-area method [38] is based upon a thermodynamic route and expresses the surface tension as a change in the free energy for an infinitesimal change in the surface area. This infinitesimal change in the area is performed throughout a perturbation process for which the perturbed system (state $A+\Delta A$) is obtained from an infinitesimal change ΔA of the area A of the reference system. The box dimensions ($L_x^{(A+\Delta A)}, L_y^{(A+\Delta A)}, L_z^{(A+\Delta A)}$) in the perturbed systems are changed using the following transformations $L_x^{(A+\Delta A)} = L_x^{(A)} \sqrt{1+\xi}$, $L_y^{(A+\Delta A)} = L_y^{(A)} \sqrt{1+\xi}$, $L_z^{(A+\Delta A)} = L_z^{(A)} / (1+\xi)$ where $\xi \rightarrow 0$. The area ($A+\Delta A$) of the perturbed state thus equals to $L_x^{(A)} L_y^{(A)} (1+\xi)$ and ΔA is equal to $L_x^{(A)} L_y^{(A)} \xi$. The operational expression for the calculation of γ within the TA method is

$$\begin{aligned} \gamma_{\text{TA}} &= \left(\frac{\partial F}{\partial A} \right)_{N,V,T} \\ &= \lim_{\xi \rightarrow 0} - \frac{k_B T}{\Delta A} \ln \left\langle \exp \left(- \frac{(U_{(A+\Delta A)}^C(\mathbf{r}'^N) - U_{(A)}^C(\mathbf{r}^N))}{k_B T} \right) \right\rangle_0 \\ &= \sum_k \lim_{\xi \rightarrow 0} - \frac{k_B T}{\Delta A} \\ &\quad \times \ln \left\langle \exp \left(- \frac{(U_{(A+\Delta A)}^C(z, \mathbf{r}'^N) - U_{(A)}^C(z, \mathbf{r}^N))}{k_B T} \right) \right\rangle_{k,A}, \end{aligned} \quad (26)$$

$\langle \dots \rangle_A$ indicates that the average is carried out over the reference state and the k slabs. $U_{(A+\Delta A)}^C(z, \mathbf{r}'^N)$ and $U_{(A)}^C(z, \mathbf{r}^N)$ are the conservative energies of the slab k in the perturbed and reference states. For the calculation of the energy, we adopt the definition of Ladd and Woodcok [56] and choose to assign in the slab centered on z two energy contributions: one contribution due to the energy between the particles within the slab and a second contribution due to the energy of the particles within the slab with those outside the slab. The energy of the slab at the position z is defined as

$$U^C(z) = \frac{1}{2} \sum_{i=1}^N H(z_i) u_i^C. \quad (27)$$

The calculation of the surface tension was carried out in the direct ($\gamma_{\text{TA,D}}$) and reverse ($\gamma_{\text{TA,R}}$) directions. The calculation of the direct direction involves an increase of the surface area ($A+\Delta A$) whereas a decrease of the surface area ($A-\Delta A$) is performed in the reverse path. The ensemble average was carried out over the configurations of the reference system whereas the configurations of the perturbed system were not included in the Markov chain of states. Thermodynamic consistency requires that the surface tension in the direct and reverse directions must be equal in magnitude and in opposite sign. This is satisfied when the configuration space of the perturbed system matches the one of the reference system. This requirement implies to use an appropriate value of ξ . The value of ξ must satisfy two constraints [38]: this value should be small enough to allow an accurate calculation of the surface tension from Eq. (26) and large enough to provide reasonable statistics for the Boltzmann factor. The surface tension value was averaged over the two directions as $(\gamma_{\text{TA,D}} - \gamma_{\text{TA,R}})/2$. We found that $\xi = 1 \times 10^{-7}$ was a good value to obtain accurate surface tension of DPD particles whereas $\xi = 1 \times 10^{-4}$ was found to be appropriate for the Lennard-Jones fluid [20,21,24,27–29,33].

V. RESULTS AND DISCUSSIONS

Figure 1(a) shows the phase envelope calculated from MDPD and MMC simulations. The coexisting densities result from fitting the density profiles to a hyperbolic tangent function of the form

$$\rho(z) = \frac{1}{2}(\rho_l + \rho_g) - \frac{1}{2}(\rho_l - \rho_g) \tanh[2(z - z_e)/d], \quad (28)$$

where ρ_l and ρ_g are the density of the liquid and vapor phases, respectively. z_e is the height of the equimolar dividing surface and d is a measure of the interfacial thickness. We observe good agreement between the MMC and MDPD methods. The maximum deviation between the calculated liquid densities is less than 1%. The density profiles, shown in Fig. 1(b), exhibit the same features, i.e., two well developed bulk liquid and vapor phases. On the scale of the figure, no difference can be observed between the density profiles calculated from MDPD and MMC. Figure 1(c) focuses on the part of the density profiles corresponding to the liquid phase. Interestingly, the profile calculated from MMC is more homogeneous than that calculated from MDPD whereas the number of time steps is sensitively the same for the two types of simulations. The small oscillations of the density profile obtained with the MDPD method indicate that the local densities of the liquid phase are faster uncorrelated in MMC than in MDPD. This establishes the MMC method as an efficient tools for the study of the interfacial properties of fluids at a mesoscopic scale.

The dependence of the surface tension with the temperature is shown in Fig. 2(a). The surface tension is then calculated using the IK definition. The maximum deviation between MMC and MDPD is observed at the highest temperatures and is less than 5%. The average deviation between the surface tensions is 2.5%. The MMC and MDPD methods are shown to give the same values values of surface

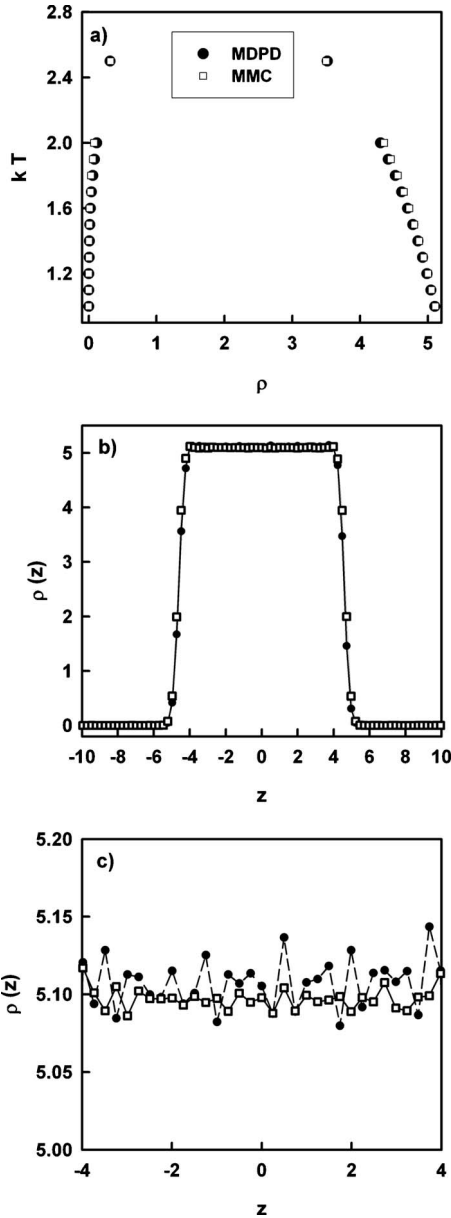


FIG. 1. (a) Phase diagram of the liquid-vapor equilibrium of DPD particles calculated from the MDPD (full circles) and MMC (open squares) simulations; (b) density profiles of DPD particles along the z axis; (c) zoom of the density profiles within the liquid bulk region.

tension. The surface tensions calculated from the KB, KBZ, and TA definitions are reported in Table I for two temperatures. Interestingly, we observe no difference between the values calculated from the mechanical and thermodynamic routes. They are equivalent within the statistical errors. Table I reports the calculation of the surface tension using the TA definition in the forward and backward directions. The values in the direct and reverse directions are equal in magnitude but in opposite signs. This indicates that the TA approach performs very well with this many-body potential. The equivalence between the surface tensions calculated on the one hand with MMC and MDPD and on the other hand with the different definitions are explained by the fact the

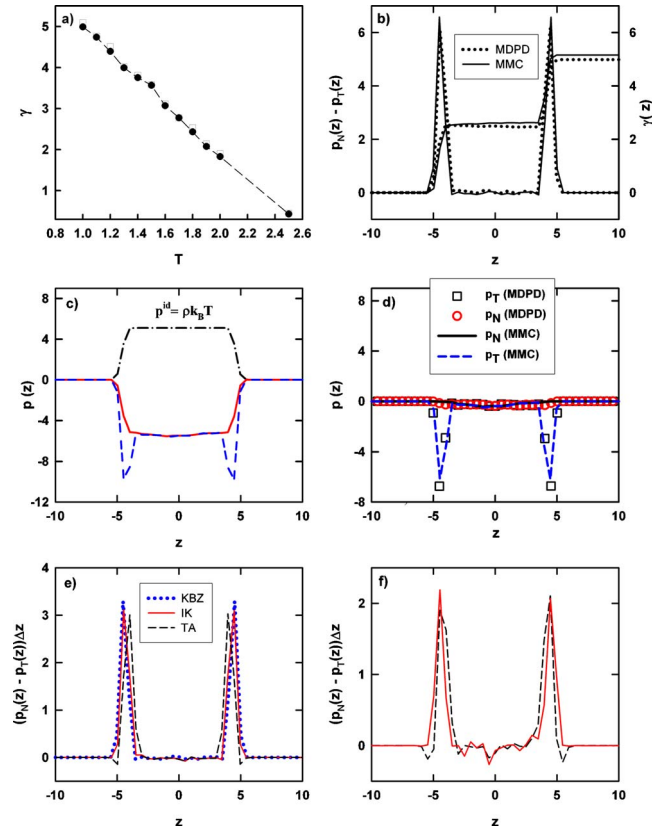


FIG. 2. (Color online) (a) Surface tension values calculated using the IK definition as a function of the reduced temperature from MDPD (full circles) and MMC (open squares) simulations; (b) profiles of the difference between the normal and tangential components of the pressure calculated using the IK definition with the MDPD and MMC methods. The integral $\gamma(z)$ of this profile is represented on the right axis for the two methods; (c) kinetic and potential parts of the normal and tangential components of the pressure tensor calculated using the MDPD and MMC simulations; (d) profiles of the normal and tangential components of the pressure tensor calculated using the MDPD and MMC simulations; (e) profiles of the difference between the normal and tangential components of the pressure calculated using the IK, TA and KBZ definitions with the MDPD and MMC simulations at $k_B T = 1.0$; (f) $p_N - p_T$ profiles calculated in the MMC simulations using the IK and TA approaches at $k_B T = 1.5$.

conservative soft potential and force are continuous at the cutoff value. This result puts the emphasis on what we have already demonstrated for the calculation of surface tension of Lennard-Jones fluids [20] from MC and MD simulations. Additionally, the use of the random and dissipative forces in the dynamics does not affect the interfacial thermodynamic properties which is in line with the correct Boltzmann distribution of the system.

The difference between the normal and tangential pressure profiles is shown in part b of Fig. 2. This $p_N - p_T$ profile allows to check that the positive peaks are well-marked and identical for the two interfaces. Their contribution to the surface tension is the same as expected for a well equilibrated system and two independent interfaces that occur in a three dimensionally periodic geometry. Even if the local value of

TABLE I. Input and configurational temperatures, surface tension values calculated from the KB, KBZ, IK, and TA definitions in the MMC and MDPD configurations. $\gamma_{\text{TA,D}}$ and $\gamma_{\text{TA,R}}$ are the surface tensions calculated with the TA approach in the direct and reverse directions, respectively. γ_A and γ_B are the contributions of the surface tension calculated using the attractive part ($A < 0$) and the many-body repulsive part ($B > 0$) of the conservative force, respectively.

T	T_{conf}	γ_{KB}	γ_{KBZ}	γ_{IK}	γ_{TA}
MMC					
1.0	1.0	5.1 ₁	5.1 ₁	5.1 ₁	5.1 ₁
1.6	1.6	3.1 ₁	3.1 ₁	3.1 ₁	3.1 ₁
MDPD					
1.0	1.0	5.0 ₁	5.0 ₁	5.0 ₁	5.0 ₁
1.6	1.6	3.1 ₁	3.1 ₁	3.1 ₁	3.1 ₁
T		$\gamma_{\text{TA,D}}$	$\gamma_{\text{TA,R}}$	γ_{TA}	
1.0		5.0 ₁	-5.0 ₁	5.0 ₁	
1.6		3.1 ₁	-3.1 ₁	3.1 ₁	
r_d		γ_A	γ_B	γ	
0.70		20.4 ₁	-10.0 ₁	10.4 ₁	
0.75		12.0 ₁	-6.9 ₁	5.1 ₁	
0.78		8.0 ₁	-4.9 ₁	3.1 ₁	

the integral of the $p_N(z) - p_T(z)$ profile can differ between the different ways of calculating the pressure components (IK, KBZ), the shape of the profile is very useful for checking the correctness of the two-phase simulation. Actually, we check from the profile of $\gamma(z)$ that the bulk liquid and vapor phases do not contribute to the surface tension. All these checks indicate that the features of liquid-vapor equilibrium are well reproduced by the multibody potential and no difference is observed between the Monte Carlo and dynamics approaches.

Part c of Fig. 2 shows the profiles of the normal and tangential components of the pressure tensor for the kinetic and potential parts. The potential part is then calculated with the IK definition using the MMC and MDPD methods. We observe that the profiles of the kinetic and potential parts are only constant in the liquid and gas bulk phases as required by the mechanical equilibrium of bulk phases. The profiles of total pressure are shown in Fig. 2(d) for the MDPD and MMC methods. The profile of the normal pressure is now constant at each z including the interfacial regions. The tangential pressure exhibits two negative peaks in the interfacial regions and is constant within the statistical fluctuations in the bulk phases. The features of these pressure profiles are identical to those calculated from Lennard-Jones interactions [20,37]. The fact that the force and potential are continuous at the cutoff radius leads to the same pressure profiles for MMC and MDPD. The difference between the normal and tangential pressure profiles is shown in part e of Fig. 2. This $p_N(z) - p_T(z)$ profile allows to check that the positive peaks are well marked and identical for the two interfaces. Their contribution to the surface tension is the same as expected for a well equilibrated system and two independent inter-

faces in the case of a three dimensionally periodic system. We also check from the profile of $\gamma(z)$ that the bulk liquid and vapor phases do not contribute to the surface tension. All these checks indicate that the features of liquid-vapor equilibrium are well reproduced by the multibody potential and no difference is observed between the Monte Carlo and dynamics approaches. The profiles confirm that the mechanical and thermodynamic routes lead to the same surface tension. The $p_N(z) - p_T(z)$ profiles are identical with the IK and KBZ approaches whereas the profile calculated from TA is slightly displaced toward the liquid phase. The peaks are slightly smaller in magnitude with TA. We also see that the region close the surface in the vapor side is characterized by the presence of negative peaks of the $p_N - p_T$ profile, suggesting a weak compression of this zone on the vapor side. The presence of this negative peak on the vapor side of the interface has been subjected to controversial discussions and depends on the method used for the calculation of the pressure tensor [20,45]. The presence of such a region of weak compression was already observed from the calculation of surface tension of Lennard-Jones fluid using Monte Carlo simulations [20] and the TA technique. However, the scalar values of the surface tension calculated from these profiles are identical for the three definitions. Figure 2(f) compares the IK and TA profiles of the $(p_N(z) - p_T(z))\Delta z$ property calculated at the reduced temperature of 1.5. Interestingly, we observe better agreement at this temperature between the IK and TA methods. The weak compression close to the surface in the vapor side is still present. Since the number of particles in the vapor side is increased at $k_B T = 1.5$, the particle density number profile is better defined. As a result, the TA calculation which is related to the presence of the delta function and

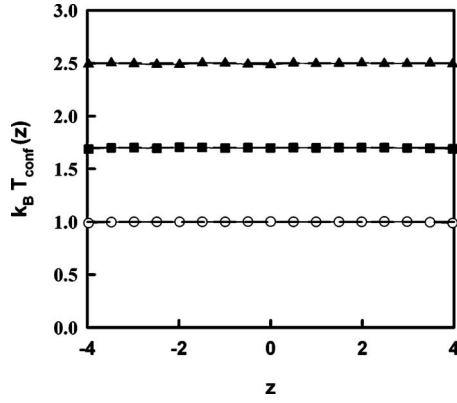


FIG. 3. Profiles of the configurational temperature calculated from MMC simulations at $k_B T=1.0$ (open circles), $k_B T=1.7$ (full squares) and $k_B T=2.5$ (full triangles) as function of z .

thus to the particle density number performs better.

Figure 3 shows the profile of the configurational temperature along the direction normal to the surface for three different temperatures. The average configurational temperature is also given in Table I. Some stages of the derivation of the configurational temperature within the multibody DPD model are given in Appendix A. First, we observe that the average configurational temperature of Table I matches exactly with the input temperature for the MMC and MDPD methods. It means that the time step used in this work ($\delta t = 0.001$) is appropriate for satisfying the canonical statistical ensemble. This was also confirmed by the calculation of the configurational temperature in standard DPD calculations [57]. Figure 3 focuses on the local configurational temperature of the liquid region calculated from MMC configurations. We check that the local configurational temperature follows exactly the input temperature within the different liquid slabs. The configurational temperature profile of the vapor phase (not shown here) is subjected to larger fluctuations and poor statistics due to the small number of DPD particles in this vapor phase. Anyway, the average configurational temperature calculated over the slabs of the simulation box is in perfect agreement with the imposed temperature.

We plot in Fig. 4(a) the profiles of the potential part of the pressure tensor calculated from the KBZ definition [Eq. (25)]. The profiles of the normal component of the pressure are represented for three different values of r_d . This cutoff radius is the range of the repulsive many-body contribution of the conservative force. The choice of the value is quite empirical and the standard version of the MDPD model [15] was derived with $r_d=0.75$. Part a of Fig. 4 shows that the profile of the potential part of the pressure calculated using KBZ exhibits two small peaks at the liquid-vapor interfaces for $r_d=0.75$ and $r_d=0.70$. The magnitude of these peaks increases with decreasing r_d values. This oscillation can disappear with larger r_d values. However, the profile of the normal component of the potential part to the pressure should be constant at each z value within the liquid phase as observed in Fig. 4(b) with the IK definition. The normal component which sums the kinetic and configurational parts of the pressure must be then constant at each z as it is checked in part c

of Fig. 4 with the IK definition for $r_d=0.70$. However, the normal pressure component calculated at $r_d=0.70$ with KBZ exhibits a positive peak and a negative peak at the interfacial region. These peaks are not compensated by the kinetic contribution. The KBZ calculation at $r_d=0.70$ is then very dependent on the density oscillations at the interface region. Interestingly, the profiles of the normal component of the potential part calculated from the IK definition do not show any oscillations close to the interfaces whatever the value of r_d . This difference between the two methods has already been reported in a previous study [53,54]. The calculation of the pressure from the KBZ or IK1 approximations is in fact strongly correlated with the local density number. It means that the differences between the KBZ and IK approaches increase with the heterogeneity in the system. This is exactly what we observe when we increase the value of r_d : increasing r_d amounts for increasing the repulsive part of the conservative force and making the liquid phase less attractive. The density gradient in the interfacial zone is then less pronounced. The profiles of the tangential part of the configurational pressure do not show in Fig. 4(d) any additional oscillations at the interfaces except the negative peak indicating that the interface is under tension. The profile of p_T is then independent of the method (IK or KBZ) used. However, the integration of the $p_N - p_T$ quantity does not depend on the definition used. The positive and negative peaks observed with the KBZ definition in the normal component cancel each other and explains why the surface tension is identical within the KBZ and IK definitions for different r_d values.

The choice of the value of r_d impacts very much on the magnitude of the negative peak of p_T . For this reason, Fig. 5 represents the contribution to the attractive and repulsive parts of the conservative force in the surface tension as a function of r_d . Table I reports the values of the surface tension calculated from the attractive and repulsive parts of the conservative force. As expected, the attractive contribution of the conservative force ($A < 0$) gives rise to a positive value of γ whereas a negative surface tension contribution is obtained from the repulsive many-body term ($B > 0$) of the conservative force. We check that the total surface tension decreases significantly with increasing r_d . The surface tension decreases from 10.4 to 1.9 when r_d increases from 0.7 to 0.8. This makes the choice of r_d very sensitive in the case of the surface tension calculation.

VI. CONCLUSIONS

The many-body soft potential model has been used through Monte Carlo (MMC) and dynamics (MDPD) methods to calculate both the coexisting densities and the surface tension of the liquid-vapor interface of DPD particles. The surface tension has been calculated from different mechanical and thermodynamic routes. We have shown that the MMC and MDPD methods lead to the same interfacial properties and coexisting densities for a given temperature. Additionally, the KB, KBZ, IK, and TA definitions of the surface tensions are consistent and give exactly the same value of surface tension. The fact that the conservative force and potential equations are continuous at the cutoff radius im-

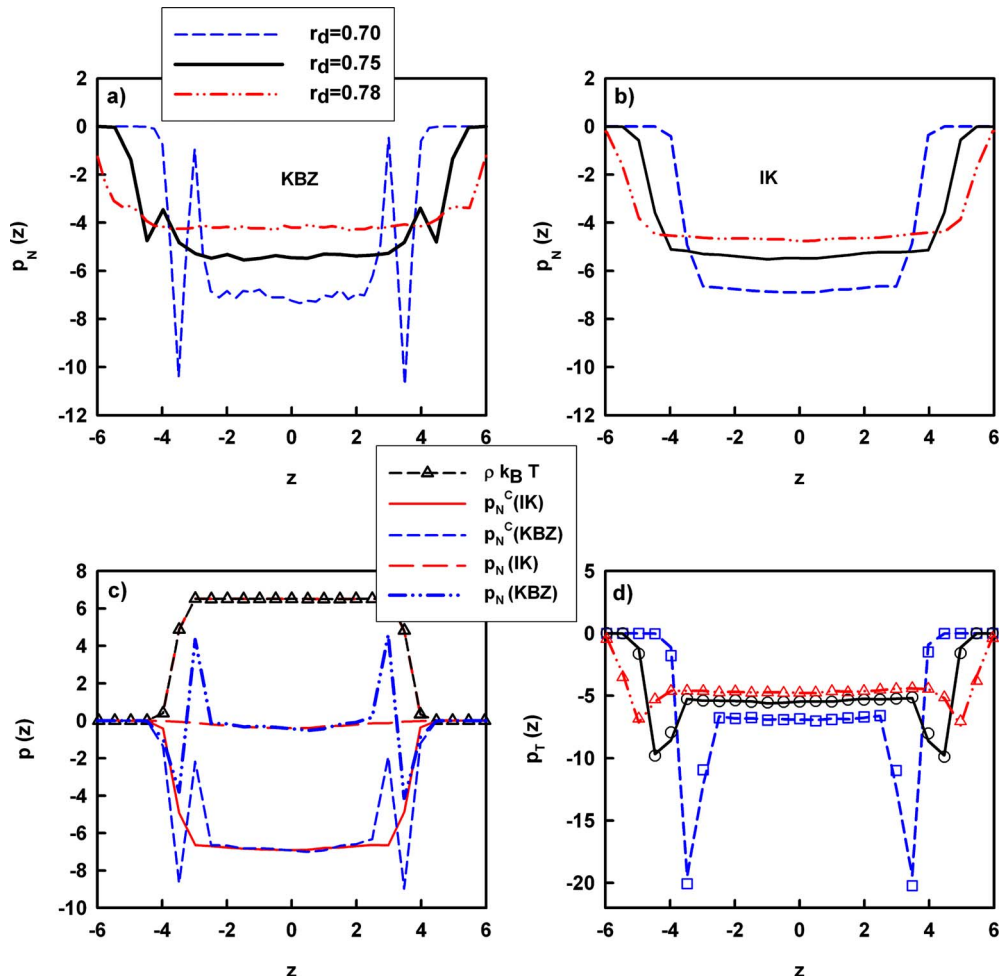


FIG. 4. (Color online) Profiles of the potential part of the normal component of the pressure tensor calculated for three r_d values using the (a) KBZ and (b) IK definitions; (c) profiles of the kinetic, potential and total parts of the normal component of the pressure tensor calculated using the IK and KBZ approaches for $r_d=0.7$; (d) profiles of the potential part of the tangential component of the pressure tensor calculated using the KBZ (open symbols) and IK (lines) for three values of r_d .

plies the equivalence between the approaches using either the potential or its derivative in the calculation of the surface tension. This also implies the perfect equivalence between the Monte Carlo (MMC) and the dissipative particle dynamics (MDPD) simulation methods for the modeling of interfacial properties. This is the first time that the test-area and KBZ approaches are applied for the surface tension calculation of DPD particles interacting with the multibody soft potential. The comparison between the different definitions of the surface tension is very useful because the conservative potential is soft and vanishes at the cutoff. As a result, no long range corrections are required.

The configurational temperature of the MDPD method is in line with the Boltzmann temperature and indicates that the relatively large time step used respects the NVT canonical ensemble. The profiles of the normal pressure show significant differences between the KBZ and IK approaches whereas the tangential part is not dependent on the method used. We have also checked that the surface tension is dependent on the range of the many-body repulsive term of the conservative force. This makes very sensitive the choice of the r_d parameter. Given that the interfacial properties has been investigated in detail with the MMC and MDPD meth-

ods, we plan to use the MDPD methodology to calculate the surface tension of real compounds by mapping the repulsive DPD parameters on atomistic parameters.

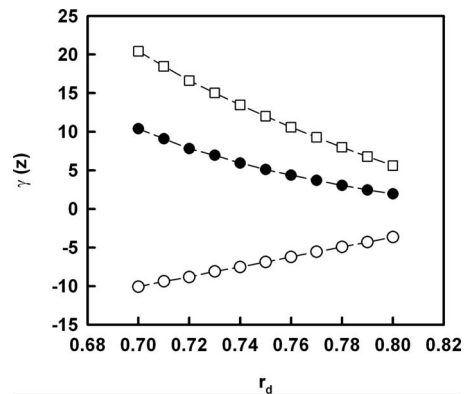


FIG. 5. Contributions to the surface tension calculated from the attractive (open squares) and many-body repulsive (open circles) parts of the conservative force as a function of r_d . The total surface tension (full circles) is represented for completeness.

ACKNOWLEDGMENTS

The authors would like to acknowledge the support of the French Agence Nationale de la Recherche (ANR) under grant SUSHI (Grant No. ANR-07-BLAN-0268) SimULATION de Systèmes Hétérogènes et d'Interfaces. This work was also granted access to the HPC resources of IDRIS under the allocation Grant No. 2009-i2009092119 made by GENCI (Grand Equipement National de Calcul Intensif).

APPENDIX A: CONFIGURATIONAL TEMPERATURE CALCULATION

The working expression of the local configurational temperature [58–61] is given by Eq. (A1) where i refers to the particles and \mathbf{F}_i is the total force acting on i . The calculations of the forces and of the derivatives with respect to the position vector are carried out by considering the attractive and repulsive part of the conservative potential of Eq. (10). The expression of the force is given in Eq. (6). The derivatives of forces are calculated using the following intermediate expressions of Eqs. (A2) and (A3).

$$k_B T_{\text{conf}}(z_k) = \frac{\left\langle \sum_{i=1, i \in k}^N \mathbf{F}_i^2 \right\rangle}{\left\langle - \sum_{i=1, i \in k}^N \left(\frac{\partial F_{ix}}{\partial r_{ix}} + \frac{\partial F_{iy}}{\partial r_{iy}} + \frac{\partial F_{iz}}{\partial r_{iz}} \right) \right\rangle} \quad (\text{A1})$$

$$\frac{\partial F_{i\alpha}^A}{\partial r_{i\alpha}} = \frac{A}{r_{ij}^2} \left(1 - \frac{r_{ij}}{r_c} \right) \left[r_{ij} \frac{\partial r_{ij\alpha}}{\partial r_{i\alpha}} - r_{ij\alpha} \frac{\partial r_{ij}}{\partial r_{i\alpha}} \right] - \frac{A r_{ij\alpha}}{r_c r_{ij}^2} \frac{\partial r_{ij}}{\partial r_{i\alpha}} \quad (\text{A2})$$

where A refers to the attractive contribution of the conservative force.

$$\begin{aligned} \frac{\partial F_{i\alpha}^B}{\partial r_{i\alpha}} = & B(\rho_i + \rho_j) \left[\frac{1}{r_{ij}^2} \left(1 - \frac{r_{ij}}{r_d} \right) \left[r_{ij} \frac{\partial r_{ij\alpha}}{\partial r_{i\alpha}} - r_{ij\alpha} \frac{\partial r_{ij}}{\partial r_{i\alpha}} \right] \right. \\ & \left. - \frac{r_{ij\alpha}}{r_d r_{ij}^2} \frac{\partial r_{ij}}{\partial r_{i\alpha}} \right] + \left(1 - \frac{r_{ij}}{r_d} \right) \frac{B r_{ij\alpha}}{r_{i\alpha}} \left[\frac{\partial \rho_i}{\partial r_{i\alpha}} + \frac{\partial \rho_j}{\partial r_{i\alpha}} \right] \end{aligned} \quad (\text{A3})$$

and B to the repulsive part of the conservative force and ρ_i is

$$\rho_i = \sum_{j \neq i} w_{ij} \quad \text{with} \quad \begin{cases} w_{ij} = \frac{15}{2\pi r_d^3} \left(1 - \frac{r_{ij}}{r_d} \right)^2 & \text{if } r_{ij} < r_d \\ 0 & \text{if } r_{ij} > r_d \end{cases} \quad (\text{A4})$$

The derivatives of ρ_i and ρ_j with respect to $r_{i\alpha}$ are obtained from Eq. (A4)

$$\frac{\partial \rho_i}{\partial r_{i\alpha}} = - \sum_{j \neq i} \frac{15}{\pi r_d^4} \left(1 - \frac{r_{ij}}{r_d} \right) \frac{\partial r_{ij}}{\partial r_{i\alpha}} \quad \text{if } r_{ij} < r_d, \quad (\text{A5a})$$

$$\frac{\partial \rho_j}{\partial r_{i\alpha}} = - \frac{15}{\pi r_d^4} \left(1 - \frac{r_{ij}}{r_d} \right) \frac{\partial r_{ji}}{\partial r_{i\alpha}} \quad \text{if } r_{ij} < r_d, \quad (\text{A5b})$$

where α represents x, y, z . $\frac{\partial r_{ij}}{\partial r_{i\alpha}}$, $\frac{\partial r_{ji}}{\partial r_{i\alpha}}$ and $\frac{\partial r_{ij\alpha}}{\partial r_{i\alpha}}$ are calculated by considering $r_{ij} = (r_{ijx}^2 + r_{ijy}^2 + r_{ijz}^2)^{1/2}$ and $r_{ij\alpha} = r_{i\alpha} - r_{j\alpha}$

-
- [1] P. J. Hoogerbrugge and J. M. V. A. Koelman, *EPL* **19**, 155 (1992).
- [2] J. M. V. A. Koelman and P. J. Hoogerbrugge, *EPL* **21**, 363 (1993).
- [3] S. H. L. Klapp, D. J. Diestler, and M. Schoen, *J. Phys.: Condens. Matter* **16**, 7331 (2004).
- [4] J. B. Avalos and A. D. Mackie, *EPL* **40**, 141 (1997).
- [5] P. Espanol, *EPL* **40**, 631 (1997).
- [6] J. B. Avalos and A. D. Mackie, *J. Chem. Phys.* **111**, 5267 (1999).
- [7] R. D. Groot, *J. Chem. Phys.* **118**, 11265 (2003).
- [8] M. Gonzalez-Melchor, E. Mayoral, M. E. Velazquez, and J. Alejandro, *J. Chem. Phys.* **125**, 224107 (2006).
- [9] C. Ibergay, P. Malfreyt, and D. J. Tildesley, *J. Chem. Theory Comput.* **5**, 3245 (2009).
- [10] C. Ibergay, P. Malfreyt, and D. J. Tildesley, *J. Phys. Chem. B* **114**, 7274 (2010).
- [11] F. Goujon, P. Malfreyt, and D. J. Tildesley, *J. Chem. Phys.* **129**, 034902 (2008).
- [12] F. Goujon, P. Malfreyt, and D. J. Tildesley, *Macromolecules* **42**, 4310 (2009).
- [13] I. Pagonabarraga and D. Frenkel, *J. Chem. Phys.* **115**, 5015 (2001).
- [14] S. Y. Trofimov, E. L. F. Nies, and M. A. Michels, *J. Chem. Phys.* **117**, 9383 (2002).
- [15] P. B. Warren, *Phys. Rev. E* **68**, 066702 (2003).
- [16] S. Y. Trofimov, E. L. F. Nies, and M. A. J. Michels, *J. Chem. Phys.* **123**, 144102 (2005).
- [17] F. Goujon, P. Malfreyt, A. Boutin, and A. H. Fuchs, *Mol. Simul.* **27**, 99 (2001).
- [18] F. Goujon, P. Malfreyt, A. Boutin, and A. H. Fuchs, *J. Chem. Phys.* **116**, 8106 (2002).
- [19] F. Goujon, P. Malfreyt, and D. J. Tildesley, *ChemPhysChem* **5**, 457 (2004).
- [20] C. Ibergay, A. Ghoufi, F. Goujon, P. Ungerer, A. Boutin, B. Rousseau, and P. Malfreyt, *Phys. Rev. E* **75**, 051602 (2007).
- [21] F. Biscay, A. Ghoufi, F. Goujon, V. Lachet, and P. Malfreyt, *J. Phys. Chem. B* **112**, 13885 (2008).
- [22] J. Janecek, H. Krienke, and G. Schmeer, *Condens. Matter Phys.* **10**, 415 (2007).
- [23] C. Nieto-Draghi, P. Bonnaud, and P. Ungerer, *J. Phys. Chem. C* **111**, 15686 (2007).
- [24] F. Biscay, A. Ghoufi, V. Lachet, and P. Malfreyt, *Phys. Chem. Chem. Phys.* **11**, 6132 (2009).

- [25] J. Alejandro, D. J. Tildesley, and G. A. Chapela, *J. Chem. Phys.* **102**, 4574 (1995).
- [26] C. Vega and E. de Miguel, *J. Chem. Phys.* **126**, 154707 (2007).
- [27] A. Ghoufi, F. Goujon, V. Lachet, and P. Malfreyt, *Phys. Rev. E* **77**, 031601 (2008).
- [28] A. Ghoufi, F. Goujon, V. Lachet, and P. Malfreyt, *J. Chem. Phys.* **128**, 154716 (2008).
- [29] A. Ghoufi, F. Goujon, V. Lachet, and P. Malfreyt, *J. Chem. Phys.* **128**, 154718 (2008).
- [30] P. Orea, J. Lopez-Lemus, and J. Alejandro, *J. Chem. Phys.* **123**, 114702 (2005).
- [31] M. Gonzalez-Melchor, P. Orea, J. Lopez-Lemus, F. Bresme, and J. Alejandro, *J. Chem. Phys.* **122**, 094503 (2005).
- [32] J. R. Errington and D. A. Kofke, *J. Chem. Phys.* **127**, 174709 (2007).
- [33] F. Biscay, A. Ghoufi, V. Lachet, and P. Malfreyt, *J. Chem. Phys.* **130**, 184710 (2009).
- [34] A. Trokhymchuk and J. Alejandro, *J. Chem. Phys.* **111**, 8510 (1999).
- [35] J. Lopez-Lemus and J. Alejandro, *Mol. Phys.* **100**, 2983 (2002).
- [36] P. Grosfils and J. F. Lutsko, *J. Chem. Phys.* **130**, 054703 (2009).
- [37] F. Goujon, P. Malfreyt, J. M. Simon, A. Boutin, B. Rousseau, and A. H. Fuchs, *J. Chem. Phys.* **121**, 12559 (2004).
- [38] G. J. Gloor, G. Jackson, F. J. Blas, and E. de Miguel, *J. Chem. Phys.* **123**, 134703 (2005).
- [39] J. G. Kirkwood and F. P. Buff, *J. Chem. Phys.* **17**, 338 (1949).
- [40] F. B. Buff, *Z. Elektrochem. Angew. Phys. Chem.* **56**, 311 (1952).
- [41] A. G. McLellan, *Proc. R. Soc. London, Ser. A* **213**, 274 (1952).
- [42] A. G. McLellan, *Proc. R. Soc. London, Ser. A* **217**, 92 (1953).
- [43] J. S. Rowlinson and B. Widom, *Molecular Theory of Capillarity* (Clarendon Press, Oxford, 1982).
- [44] J. H. Irving and J. G. Kirkwood, *J. Chem. Phys.* **18**, 817 (1950).
- [45] J. P. R. B. Walton, D. J. Tildesley, J. S. Rowlinson, and J. R. Henderson, *Mol. Phys.* **48**, 1357 (1983).
- [46] J. P. R. B. Walton, D. J. Tildesley, and J. S. Rowlinson, *Mol. Phys.* **58**, 1013 (1986).
- [47] M. Guo and B. C. Y. Lu, *J. Chem. Phys.* **106**, 3688 (1997).
- [48] V. K. Shen, R. D. Mountain, and J. R. Errington, *J. Phys. Chem. B* **111**, 6198 (2007).
- [49] P. Espanol and P. B. Warren, *EPL* **30**, 191 (1995).
- [50] M. E. Velazquez, A. Gama-Goicochea, M. Gonzalez-Melchor, M. Neria, and J. Alejandro, *J. Chem. Phys.* **124**, 084104 (2006).
- [51] P. Schofield and J. R. Henderson, *Proc. R. Soc. London, Ser. A* **379**, 231 (1982).
- [52] J. P. R. B. Walton and K. E. Gubbins, *Mol. Phys.* **55**, 679 (1985).
- [53] B. D. Todd, D. J. Evans, and P. J. Daivis, *Phys. Rev. E* **52**, 1627 (1995).
- [54] F. Varnik, J. Baschnagel, and K. Binder, *J. Chem. Phys.* **113**, 4444 (2000).
- [55] A. Harasima, *Adv. Chem. Phys.* **1**, 203 (1958).
- [56] A. J. C. Ladd and L. V. Woodcock, *Mol. Phys.* **36**, 611 (1978).
- [57] M. P. Allen, *J. Phys. Chem. B* **110**, 3823 (2006).
- [58] H. H. Rugh, *Phys. Rev. Lett.* **78**, 772 (1997).
- [59] O. G. Jepps, G. Ayton, and D. J. Evans, *Phys. Rev. E* **62**, 4757 (2000).
- [60] G. Rickayzen and J. G. Powles, *J. Chem. Phys.* **114**, 4333 (2001).
- [61] J. Delhommelle and D. J. Evans, *J. Chem. Phys.* **114**, 6229 (2001).